Journal Pre-proofs

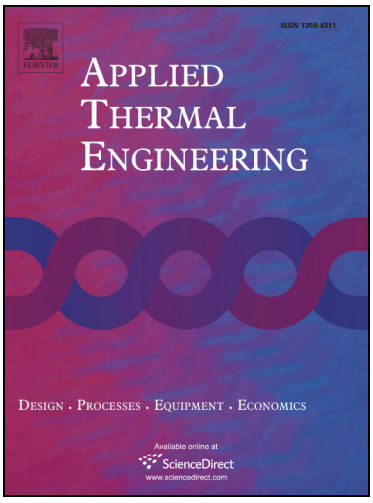

Simulation of an Aircraft Environmental Control System

Ian Jennions, Fakhre Ali, Manuel Esperon Miguez, Ignacio Camacho Escobar

PII: S1359-4311(19)35081-1
DOI: https://doi.org/10.1016/j.applthermaleng.2020.114925
Reference: ATE 114925

To appear in: *Applied Thermal Engineering*

Received Date: 23 July 2019
Revised Date: 28 November 2019
Accepted Date: 8 January 2020

Please cite this article as: I. Jennions, F. Ali, M. Esperon Miguez, I. Camacho Escobar, Simulation of an Aircraft Environmental Control System, *Applied Thermal Engineering* (2020), doi: https://doi.org/10.1016/j.applthermaleng.2020.114925

Applied Thermal Engineering, Volume 172, May 2020, Article number 114925
DOI: 10.1016/j.applthermaleng.2020.114925

Simulation of an Aircraft Environmental Control System

Ian Jennions[a,]i.jennions@cranfield.ac.uk, **Fakhre Ali**[b,*,]f.ali@cranfield.ac.uk, **Manuel Esperon Miguez**[c,]manuel.esperon@jci.com, **Ignacio Camacho Escobar**[d,]ignacio.camachoescobar@altran.com

[a]Integrated Vehicle Health Management Centre, School of Aerospace, Transport & Manufacturing, Cranfield University, Bedfordshire, MK430AL, UK

[b]Integrated Vehicle Health Management Centre, School of Aerospace, Transport & Manufacturing, Cranfield University, Bedfordshire, MK430AL, UK

[c]Johnson Controls International, Sunbury-on-Thames, TW16 5DB, UK.

[d]Wind Consultant Engineer, Altran-EILiS (Energy, Industry & Life Sciences)

[*]Corresponding author.

Highlights

Development of a cost effective aircraft environmental control system simulation framework.

Verification and validation of Boeing 737-800 passenger air conditioner at component level.

The quantification of ram air impact on the performance of the aircraft environmental control system.

Abstract

The environmental control system of a civil aircraft is a major driver of maintenance. Legacy systems, such as those on the Boeing 737, are particularly at risk, as they are not instrumented for health management. These systems degrade in operation and allow compensation within their operation for degrading components, until severe degradation or failure results. The required maintenance is then both costly and disruptive. The goal of this research is to produce a simulation environment that can model the aircraft environmental

control system, in order that analysis for sensor placement and algorithms can be performed without extensive, and expensive, testing. A simulation framework called Simscape Environmental Control System Simulation under All Conditions has been proposed and implemented. It offers a library of components that can be assembled into specific aircraft environmental control system simulation configurations. It is capable of simulating the health state indicating parameters at sub-system and component levels under a wide-range of aircraft operating scenarios. The developed framework has been successfully implemented to simulate a Boeing 737-800 passenger air conditioner. Its verification and validation has been carried out against the actual data corresponding to a Boeing 737-800 passenger air conditioner operating at two different cruise operating points. An extensive comparison of the simulation is presented against the data for all the passenger air conditioner components. The overall acquired results suggest that changes in the aircraft ambient conditions can have a noticeable impact on the demanded passenger air conditioner outlet temperature, and a substantial impact on the heat transfer in the primary and secondary heat exchangers. The reported simulation capability serves as a first step towards formulating an environmental control system fault simulation and diagnostic solution.

Highlights

- *Development of a cost effective aircraft environmental control system simulation framework.*
- *Verification and validation of Boeing 737-800 passenger air conditioner at component level.*
- *The quantification of ram air impact on the performance of the aircraft environmental control system.*

Nomenclature

Acronyms	
Alt	Altitude (m)
ACS	Air Cycle System
ACM	Air Cycle Machine
ADS	Air Distribution System
AIS	Anti-Ice System

BAS	Bleed Air System
B737	Boeing 737
CO	Compressor Outlet
C*O*	Water content
CHX	Condenser
CHX_O	Condenser Outlet
CPCS	Cabin Pressure Control System
ECS	Environmental Control System
HX	Heat Exchanger
HPWS	High Pressure Water Separator
MO	Merge Outlet
MMS	Mixing Manifold System
Mach	Mach number
PACK	Passenger Air Conditioner
PO	PACK Outlet
PID	Proportional Integral Derivative
PV	PACK Valve
PVO	PACK Valve Outlet
PVI	PACK Valve Inlet
PVIP	PACK Valve Inlet Pressure (kPa)
PVOP	PACK Valve Outlet Pressure (kPa)
PHX	Primary Heat Exchanger
PHXO	Primary Heat Exchanger Outlet
RC	Reference Case
RH	Relative Humidity (%)
SESAC	Simscape ECS Simulation under All Conditions
SH	Specific Humidity (kg/kg)
SHS	Specific Humidity at Saturation (kg/kg)
SHX	Secondary Heat Exchanger
SHXO	Secondary Heat Exchanger Outlet
T_I	Turbine Inlet
TCV	Temperature Control Valve
V&V	Validation & Verification
VCS	Vapour Cycle System
WS	Water Separator
WSO	Water Separator Outlet
Subscript	
P	Pressure (kPa)
T	Temperature (K)
T_{amb}	Ambient Temperature (K)
T_{hi}	Hot side inlet temperature (K)
Th_o	Hot side outlet temperature (K)
T_{ci}	Cold side inlet temperature (K)
T_{co}	Cold side outlet temperature (K)
P_{hi}	Hot side inlet Pressure (kPa)
P_{ho}	Hot side outlet Pressure (kPa)
P_{amb}	Ambient Pressure (kPa)

D_H	Hydraulic diameter (m)
D_{Hh}	Hydraulic diameter hot side (m)
D_{Hc}	Hydraulic diameter cold side (m)
f_h	Friction coefficient hot side
f_c	Friction coefficient cold side
C_d	Discharge coefficient
C_p	Specific heat of air and water vapour mixtures-Pressure (J/Kg. K)
C_v	Specific heat of air and water vapour mixtures-Volume (J/Kg. K)
C_{pw}	Specific heat of water vapour
C_{pa}	Specific heat of air
C_{plw}	Specific heat of liquid water
L_h	Length hot side (m)
L_c	Length cold side (m)
K_C	Geometric factor cold side
K_h	Geometric factor hot side
PR_c	Compressor pressure ratio
PR_t	Turbine pressure ratio
N_c	Compressor rpm
N_t	Turbine rpm
N	ACM rpm
R_a	Specific gas constant of air (J/kg. K)
R_w	Specific gas constant of water vapour (J/kg. K)
T_{wb}	Wet bulb temperature (K)
T_{dp}	Dry bulb temperature (K)
T_{BAS}	Bleed air temperature (K)
P_{BAS}	Bleed air pressure (kPa)
h	Local heat transfer coefficient (W/m^2)
P_{ws}	Partial pressure of water vapour at saturation (Pa)
m_w	Mass of the water vapour present in the moist air (kg)
m_a	Mass of the dry air (kg)
P_{Cab}	Cabin pressure (kPa)
T_{Cab}	Cabin temperature (K)
$\dot{m}_{Cab}$	Cabin mass flow (kg/s)
Greek Symbols	
$\dot{m}$	Mass flow (kg/s)
$\dot{m}_c$	Cold mass flow (kg/s)
$\dot{m}_h$	Hot mass flow (kg/s)
$\dot{m}_{ci}$	Cold side inlet mass flow (kg/s)
$\dot{m}_{co}$	Cold side outlet mass flow (kg/s)
ϵ	Effectiveness (%)
ϵ_{maps}	Effectiveness from the maps (%)
ρ_h	Density hot side (kg/m^3)

v_h	Fluid velocity hot side (m/s)
γ	Ratio of specific heats $= C_p/C_v$
η_c	Compressor isentropic efficiency (%)
η_t	Turbine isentropic efficiency (%)
η_m	Mechanical efficiency of the AMS (%)
ΔP	Pressure drop (%)
ΔT	Temperature drop (%)
$\dot{W}_c$	Compressor power (W)
$\dot{W}_t$	Turbine power (W)

1. Introduction

The Environmental Control System (ECS) is responsible for two key functions: (i) provide pressurised air to the anti-ice system and Passenger Air Conditioner (PACK), and: (ii) regulate cabin temperature, pressure (T, P) and humidity [1]. It is required to deliver these functions throughout the aircraft operational envelope. This envelope ranges from high altitude flight conditions with very low pressure, temperature, and humidity, to taxing in a tropical airport with high temperature and humidity.

The ECS on legacy aircraft such as the Boeing 737 is equipped with limited sensors and therefore provides little technical data to support the implementation of a health management strategy in order to efficiently diagnose and isolate critical faults. Furthermore, the incorporated temperature and flow control valves have the capability to mask potential faults, making the diagnostics process even more formidable. Therefore, the ECS has been reported as one of the key unscheduled maintenance drivers by the operators [2].

The aviation industry is currently proactively exploring predictive maintenance approaches that allow real-time monitoring of key systems, sub-systems and components [2-5]. In the context of the ECS, this necessitates the requirement to equip the system with appropriate condition monitoring capabilities. Correct placement of health monitoring sensors is crucial for the proper operation of a health monitoring system. A first step in determining correct sensor placement and diagnostic solutions involves accurate performance simulation of the system being monitored. To do this, the performance characteristics of the ECS at sub-system and component levels need to be well understood under a wide-range of aircraft

operating scenarios. The existing literature provides component level and system level analyses of the ECS, however, it lacks a systematically verified and validated ECS simulation tool and data at sub-system and component level in terms of pressure, temperature and mass flow. In this study, an ECS simulation tool has been proposed and validated against experimental data at sub-system and component level. The reported simulation capability serves as a first step towards formulating an ECS fault simulation and diagnostics solution.

1.1 Description of the ECS

The overall ECS is composed of several sub-systems, illustrated in Fig. 1, which are:

- Bleed Air System (BAS)
- Anti-Ice System (AIS)
- PACK
- Mixing Manifold System (MMS)
- Air Distribution System (ADS)
- Cabin Pressure Control System (CPCS)

As shown in Fig. 1 the BAS provides pressurised air to the AIS and the PACK from the main engines. During ground operation bleed air is supplied by the on-board Auxiliary Power Unit (APU) and is extracted from the main engine compressor when the aircraft is in flight. The output of the PACK is the conditioned air, which is supplied to the cabin through the mixing manifold and air distribution system.

Figure 2 illustrates the PACK as a key sub-system responsible for conditioning the bleed air. There are normally two PACKs in most narrow and wide-body civil aircraft, both PACKs are generally installed in parallel on either side of the airplane centreline, on the underside of the fuselage. Each PACK is composed of components such as Heat Exchangers (HXs), an Air Cycle Machine (ACM), a High Pressure Water Separator (HPWS) as well as flow and temperature control valves. The functionality of these components enables the PACK to condition the pressure, temperature and humidity content of the bleed air to match the requirements imposed by the cabin zone controllers. Input to these controllers is given by the flight crew from the Flight Deck (FD) based on crew feedback from each cabin zone.

Once the air has been conditioned in the PACK, it is supplied to the MMS, where it is mixed with recirculated cabin air, the recirculated air helps to alleviate the overall load requirement on the PACKs. The MMS supplies the conditioned air to the dedicated cabin zones through the ADS, enabling the aircraft to maintain a safe and comfortable flight environment. Finally, the role of the CPCS is to regulate the pressure throughout the cabin,

this is achieved through the adjustment of a set of pressure release valves, controlled directly from the FD.

From Fig. 2 the PACK can be treated as an integrated system, taking bleed air as input and generating conditioned air against the required T, P as an output, satisfying the demanded environmental requirements of the cabin. In order to propose safe and efficient ECS solutions, understanding the performance characteristics of the PACK throughout the aircraft operational envelope is necessary. Aligning this with the operator's interest to optimise maintenance activities across the aircraft systems compels requirements to:

(i) Advance the level of scientific understanding towards how the PACK and its component's useful life degrades under a wide-range of operating scenarios.
(ii) The quantification of the level of impact the sub-system and component level performance interdependencies have towards determining the optimum functionality of the PACK.
(iii) Identification and quantification of the sub-system and component health state indicating parameters needed in order to conceive new diagnostic and prognostic solutions.

These requirements have led to research initiatives [6-13] dedicated towards the sub-system and component level performance assessment of the PACK and its condition monitoring throughout the aircraft operational envelope. The PACK has become an active area of research, collaboratively addressed by academia and aircraft original equipment manufacturers. It is strongly driven by the quest to propose innovative retrofit health management solutions for legacy aircraft.

The development of a simulation framework targeting the detail design and performance assessment of the PACK therefore serves as a prerequisite in order to support the aforementioned requirements. The simulation framework must support the system, sub-system and component level modelling of the PACK. The modelling fidelity must capture the PACK performance characteristics as well as the impact of the sub-system and component level performance interdependencies on the overall system. The tool must be computationally efficient and provide a user friendly simulation environment, with the flexibility to model multiple PACK configurations under healthy and faulty operating scenarios.

1.2 Aircraft air conditioning system

Most legacy and modern civil aircraft employ an air cycle type air conditioning system. These make use of engine bleed air or APU pneumatic air as the source of air. The heart of such a system is the refrigeration turbine unit, also known as the ACM. It is comprised of a compressor that is driven by a turbine on a common shaft. The ACM unit is mounted in the PACK along with heat exchangers, water separator and control valves. Figure 3 illustrates the B 737-800 PACK architecture and shows the air flow through it.

The bleed air is supplied to the PACK at high temperature and pressure. Using the ram air as a heat sink, the PACK removes heat from the air flow in the primary and secondary HXs, reduces its pressure and temperature through the turbine incorporated in the ACM, and extracts water using a HPWS in order to comply with the demanded cabin environment requirements. There are several types of PACK configurations, however most PACKs installed in civil aircraft are very similar in terms of their design architecture. The input bleed air is regulated by a butterfly type flow control valve, labelled as the PACK Valve (PV) in Fig. 3. The total amount of air entering the PACK is first split into two streams: one will remain hot while the other will be cooled down. Both are remixed further downstream to achieve the demanded target outlet temperature, a process regulated using the Temperature Control Valve (TCV). To create the cold stream, input bleed air passes through a Primary Heat Exchanger (PHX) where it is cooled down. The flow is then compressed using a centrifugal compressor, cooled again in the Secondary Heat Exchanger (SHX), and is subsequently expanded using a turbine. This compression-expansion process improves the effectiveness of the SHX, and is conveniently performed by a single unit in which the compressor and the turbine are mounted on the same shaft. This component is called the ACM and its operation is similar to an automotive turbocharger in that it uses the work created by the turbine to drive the compressor. The expansion in the turbine often results in output temperatures below the dew point. To prevent liquid water from reaching the cabin or avionics, every PACK employs some type of water separation system. Low-pressure water separation systems use a coalescer to trap water droplets and prevent them from flowing into downstream systems. A HPWS is composed of a series of HXs to force condensation and extract liquid water before air enters the turbine. The later approach is more effective and has replaced low pressure systems in modern aircraft. Whilst some aircraft use more complex designs to increase the efficiency and/or effectiveness of the process, they tend to use a combination of the same components: HXs, ACM, WS, and valves.

1.3 Existing ECS simulation frameworks

The Functional Model Library of the Environmental Control System (FLECS) is a simulation tool, which is composed of an ECS component library [14]. Each component is taken as an individual module and is formulated based on thermodynamics and control system logic. C. Muller et al. [15] employed FLECS to conduct a dynamic simulation of the ECS, focusing primarily on the response characterises of the trim values within the air distribution ducts for a range of cabin target temperatures. For Verification and Validation (V&V), temperature readings based on the flight test of an A340-600 at the inlet of the supply duct, inlet of the cabin, and at two different cabin zones were used. In terms of the PACK performance characteristics, only mass flow at PACK outlet was simulated to support target temperature adjustment. The acquired results for the temperature profile in the cabin demonstrated good correlation with the flight test data. FLECS has not been employed to model the performance characteristics of the PACK at sub-system and component level.

Flowmaster is a 1-D thermo-fluid systems simulation tool capable of simulating an ECS [16]. Tu, Y. et al. [17] implemented a PACK model in Flowmaster. Their work was focused on the modelling of the cabin temperature control system based on the deployment of a Proportional Integral Derivative (PID) controller. Furthermore, they took into consideration the effect of the specific humidity of the flow to model the HX and ACM. The simulation results were validated against experimental data with maximum and minimum deviation of 4.3 ℃ and 0.2 ℃, the model V&V did not include the pressure and mass flow readings throughout the system. Lang X. et al. [18] deployed Flowmaster for fault detection in pipes, simulations were focused on simulating the pipe leakage based on the pressure signal.

The Boeing Company developed EASY5 software, targeting an integrated simulation modelling capability that can be employed to create both nonlinear and linearized analyses of

the ECS system [19]. The library was developed based on a modular modelling concept. Easy5 also supports the creation of additional components using Fortran. The user is required to organise the components to be placed according to a reference ECS configuration. The desired model and the interconnection between the components are formed by the built-in model generation program, which supports generating a schematic diagram of the target architecture.

EASY5 was later used by Boeing for developing an aircraft PACK model for performance analysis and for sub-systems level diagnostics. Following that, Hoffman et al. [20] reported a study that deployed EASY5 for the simulation of the F-14 fighter aircraft ECS. In another study Gulfstream Aerospace used this software to develop a PACK model for the G500 and G550 passenger jets [21]. The SAAB Group collaborated with Linköping Institute of Technology to model a PACK for their JAS39 Gripen fighter jet [22]. Fault modes identified from historic data, focussing mostly on valve jamming, were used to develop a model based diagnostic method. The overall research was however focused on validation of an existing sensor set, and was predominantly based on ground static test data.

Romani R. et al. [23] programmed a Cabin Temperature Control (CTC) model using a Mathworks developed simulation environment called Simulink. The validation of the model has been conducted using the test data under different aircraft operating conditions: cabin cooling in flight, cabin heating in flight. Their results correlated well with the data. Their analysis lacks the modelling of the PACK flow control and temperature control valve responses that have the potential to mask fault symptoms and therefore the ability to manipulate the actual performance characteristics of the sub-systems and components.

Based on the review of the existing simulation frameworks, it is noted that the existing public domain literature lacks:

1. A flexible, easy to use, ECS simulation tool, capable of modelling the sub-system and component level performance characteristics of an ECS under a wide-range of aircraft operating scenarios.
2. A systematically developed PACK model and the validation and verification of its component level performance characteristics.

1.4 Scope of present work

In this paper a sub-system and component level ECS simulation tool called SESAC (Simscape ECS Simulation under All Conditions) is reported. SESAC offers a library of

components that can be assembled to model the PACK. It is capable of simulating the health state indicating parameters of the PACK throughout the aircraft operational envelope and under a wide-range of operating scenarios. For successful demonstration of SESAC within this study, the developed library has been used to model a Boeing 737-800 (B737-800) PACK. For brevity, only the components necessary for this simulation are detailed in this paper. For the V&V of the developed PACK simulation, two Reference Cases (RCs) have been employed, representing actual data from a B737-800 PACK at two different cruise operating points. An extensive comparison of the simulation is presented against the data for all the PACK components. The component performance characteristics are discussed in detail and their interdependencies are highlighted. The impact of ambient conditions on the PACK boundary conditions and component level performance is also presented and discussed.

The remaining paper reports on the employed simulation methodology, verification and validation methodology, and comparison of simulation results against the data. The employed component equations, and PACK model development is discussed under the simulation methodology section. The acquired overall model average errors against the data and the component level performance V&V of the developed simulation are reported under the results and discussion section.

2. Simulation Methodology

This section reports on the methodology employed for the modelling and simulation of the PACK. First, the components necessary for the modelling of the PACK are presented in terms of the equations for pressure, temperature and mass flow in section 2.1. Subsequently, the treatment of humidity is outlined in section 2.2. Section 2.3 details the simulation environment. In section 2.4 and 2.5 PACK model development and the respective boundary conditions are addressed.

2.1 Formulation of the components

The components necessary to model a B737-400 ECS are:

- Valves
- HXs

- Compressor, Turbine, and Shaft, combined as an ACM
- Merge
- WS

For each component, equations for: *T, P, and ṁ* are needed, and are detailed below.

2.1.1 Valves

Valves are used on the ECS to accomplish flow control, pressure regulation, and temperature control. There are many different valves in an ECS, here they are all simulated using equation 1 [24]:

$$\dot{m} = \frac{K\, C_d\, A\, N\, P_1}{\sqrt{T_1}} \quad (1)$$

The butterfly valve is the most common type of valve used in the aircraft ECS. The valve cross section is circular and the geometric area of the valve is given by equation 2, where D is the diameter and θ is the opening angle:

$$A = \frac{\pi D^2}{4}(1 - cos\theta) \quad (2)$$

The modelling of a butterfly valve can be summarized as follows:

Temperatures	$T_1 = T_2$
Pressures	$P_1 \rightarrow Inputs$
Mass flow rate	$\dot{m}_1 = \dot{m}_2$
Specific humidity	$SH_1 = SH_2$
Liquid water content	$CO_1 = CO_2$

2.1.2 Heat Exchanger

There are normally five types of heat exchangers in an ECS (pre-cooler, primary and secondary heat exchangers, reheater, and condenser), with only the last four appearing in the PACK, see Fig. 3.

Heat exchangers come in many forms, characterized by the circulation pattern of the hot and cold air streams. In the B737-800 cross-flow heat exchangers, where hot and cold flows are directed through channels orthogonal to each other, are used. The modelling of a heat exchanger can be summarised as follows:

- Temperatures

$$T_{ho} = T_{hi} - \frac{\varepsilon(\dot{m}C_p)_{min}(T_{hi} - T_{ci})}{(\dot{m}C_p)_h} \quad (3)$$

$$T_{co} = [\dot{m}_h(T_{hi} - T_{ho}) + \dot{m}_c T_{ci}]/\dot{m}_c \quad (4)$$

- Pressures (From Darcay-Weisbach [25])

$$P_{hi} - P_{ho} = f_h \frac{L_h \rho_h v_h^2}{D_{Hh} \ 2} \quad (5)$$

$$P_{ci} - P_{co} = f_c \frac{L_c \rho_c v_c^2}{D_{Hc} \ 2} \quad (6)$$

Mass flow rate	$\dot{m}_{hi} = \dot{m}_{ho}$	$\dot{m}_{ci} = \dot{m}_{co}$
Specific humidity	$SH_{hi} = SH_{ho}$	$SH_{ci} = SH_{co}$
Liquid water content	$CO_{hi} = CO_{ho}$	$CO_{ci} = CO_{co}$

The effectiveness (ε) is expressed as a map, attached to each heat exchanger. The effectiveness actually used in the map is expressed as follows:

$$\varepsilon_{maps} = \frac{\varepsilon(\dot{m}C_p)_{min}}{(\dot{m}C_p)_h} \quad (7)$$

So

$$T_{ho} = T_{hi} - \varepsilon_{maps}(T_{hi} - T_{ci}) \quad (8)$$

In addition, pressure losses coefficients have been simplified by gathering geometric factors in a unique parameter as shown below:

$$K_h = f_h \frac{L_h}{D_{Hh}} \quad K_c = f_c \frac{L_c}{D_{Hc}} \quad (9)$$

So

$$P_{hi} - P_{ho} = \frac{1}{2\rho_h}\left(\frac{\dot{m}}{K_h}\right)^2 \quad (10)$$

$$P_{ci} - P_{co} = \frac{1}{2\rho_c}\left(\frac{\dot{m}}{K_c}\right)^2 \quad (11)$$

2.1.3 Air Cycle Machine

The ACM conditions the high-pressure bleed air extracted from the engine compressor or Auxiliary Power Unit (APU) supplied to aircraft. The cold air is generated by the turbine expansion and its heat energy is converted into shaft work which is used to drive the compressor. In this work the ACM is assumed to be adiabatic i.e. no heat exchange between the fluid and the outside. The compressor is driven by the turbine expansion force so that the engine bleed air is compressed to a high pressure.

Compressor

The isentropic efficiency of a compressor is defined as the ratio of the actual work divided by the ideal work as shown below.

$$\eta_c = \frac{h_{2i} - h_1}{h_2 - h_1} = \frac{T_{2i} - T_1}{T_2 - T_1} \quad (12)$$

$$\frac{T_{2i}}{T_1} = \left(\frac{P_2}{P_1}\right)^{\frac{\gamma-1}{\gamma}} = (PR_c)^{\frac{\gamma-1}{\gamma}} \quad (13)$$

The actual outlet temperature and the compressor power can be expressed as follows using the above equations.

$$T_2 = T_1\left\{1 + \frac{1}{\eta_c}\left[(PR_c)^{\frac{\gamma-1}{\gamma}} - 1\right]\right\} \quad (14)$$

$$\dot{W}_c = \dot{m}C_p(T_2 - T_1) = \frac{\dot{m}C_pT_1}{\eta_c}\left[\left(\frac{P_2}{P_1}\right)^{\frac{\gamma-1}{\gamma}} - 1\right] \quad (15)$$

The modelling of the compressor can be summarized as follows:

Temperatures	$T_2 = T_1\left\{1 + \frac{1}{\eta_c}\left[(PR_c)^{\frac{\gamma-1}{\gamma}} - 1\right]\right\}$
Pressures	$P_2 = P_1 \cdot PR_c$
Mass flow rate	$\dot{m}_1 = \dot{m}_2$
Specific humidity	$SH_1 = SH_2$
Liquid water content	$CO_1 = CO_2$

The pressure ratio (PR_c) and the efficiency (η_c) come from compressor maps against mass flow and shaft speed.

Turbine

The isentropic efficiency of a turbine takes into consideration those differences between the ideal and the actual process. It is defined as the ratio of the actual and ideal work delivered between the same inlet and exit pressures.

$$\eta_t = \frac{h_1 - h_2}{h_1 - h_{2i}} = \frac{T_1 - T_2}{T_1 - T_{2i}} \quad (16)$$

$$\frac{T_{2i}}{T_1} = \left(\frac{P_2}{P_1}\right)^{\frac{\gamma-1}{\gamma}} = \left(\frac{1}{PR_t}\right)^{\frac{\gamma-1}{\gamma}} \quad (17)$$

The actual outlet temperature and the turbine power can be expressed as follows using the above equations.

$$T_2 = T_1\left\{1 - \eta_t\left[1 - \left(\frac{P_2}{P_1}\right)^{\frac{\gamma-1}{\gamma}}\right]\right\} \qquad (18)$$

$$\dot{W}_t = \dot{m}C_p(T_1 - T_2) = \dot{m}C_pT_1\eta_t\left[1 - \left(\frac{P_2}{P_1}\right)^{\frac{\gamma-1}{\gamma}}\right] \qquad (19)$$

The modelling of the turbine cam be summarized as follows:

Temperatures	$T_2 = T_1\left\{1 - \eta_t\left[1 - \left(\frac{P_2}{P_1}\right)^{\frac{\gamma-1}{\gamma}}\right]\right\}$
Pressures	$P_2 = {P_1}/{PR_t}$
Mass flow rate	$\dot{m}_1 = \dot{m}_2$
Specific humidity	$SH_1 = SH_2$
Liquid water content	$CO_1 = CO_2$

The pressure ratio and efficiency for a specific operating point are obtained by using maps in a similar way to the compressor.

Shaft

The shaft is the common component between the turbine and the compressor in the ACM. Thus, the rotational speed (N) of these components is the same. The air expansion in the turbine generates the turbine power that it is used to compress the air in the compressor. However, the maximum turbine power that can be transmitted is usually constrained by several losses. The mechanical efficiency (η_m) measures the effectiveness with which the ACM performs.

- ACM matching

$$\dot{W}_t = \eta_m\dot{W}_c \qquad (20)$$

- Rotational speed

$$N_t = N_c = N \qquad (21)$$

Note that some ACMs could have also a fan joined to the same shaft. In that case, the fan contribution should be taken into account including fan power in the energy balance. In this study ACM components have been coded as a compact component, i.e. compressor, turbine

and shaft together as one unique block. This block facilitates the matching procedure of the ACM based on bleed air characteristics, compressor performance maps, turbine performance maps and shaft equations in which compressor and turbine rotational speed and powers are correlated.

2.1.4 Merge

The modelling of a merge can be summarized as follows:

- Temperatures

$$h_1 + h_2 = h_3 \quad (22)$$

- Pressures

$$P_1 = P_2 = P_3 \quad (23)$$

- Mass flow rate

$$\dot{m}_1 + \dot{m}_2 = \dot{m}_3 \quad (24)$$

- Specific humidity

$$\dot{m}_1 SH_1 + \dot{m}_2 SH_2 = \dot{m}_3 SH_3 \quad (25)$$

- Liquid water content

$$\dot{m}_1 CO_1 + \dot{m}_2 CO_2 = \dot{m}_3 CO_3 \quad (26)$$

The subscripts refer to inlet 1(1) and inlet 2 (2) and exit (3) respectively.

2.1.5 Water Separators

In earlier versions of the B737 low pressure water separator (LPWS) were used but, for efficiency and reliability, high pressure water separators (HPWS) became favoured. HPWS are essentially heat exchangers in which the temperature of the hot air is reduced below the dew point temperature, thus resulting in condensation of vapour. They are usually located upstream of the expansion turbine. Because the air velocity in the exchanger core is relatively low, the bulk of the condensate forms films or droplets on the heat exchanger surfaces. This water is swept up by the air stream to the heat exchanger outlet where it is collected by the water separator.

In the water separator, thermal effects are not considered due to the temperature difference between the fluid and the ambient being relatively small; the water separator housing is considered as adiabatic. The drop in the total pressure of the flowing gas is given by:

$$\Delta P = \frac{1}{2\rho} \cdot \left(\frac{\dot{m}}{K}\right)^2 \quad (27)$$

Where K is constant that relates geometry parameters and flow conditions through the water separator, ρ is the air density and $\dot{m}$ is the mass flow rate. The liquid water content removed in the water separator is calculated using the water removal efficiency as follows:

$$CO_2 = \eta \cdot CO_1 \qquad \text{Eq. 28}$$

Once the above variables have been calculated the humidity routine is applied to recalculate, if necessary, the outlet temperature and the outlet specific humidity.

The modelling of a water separator can be summarized as follows:

Temperatures	$T_1 = T_2$
Pressures	$P_2 - P_1 = \frac{1}{2\rho} \cdot (\frac{\dot{m}}{K})^2$
Mass flow rate	$\dot{m} = \dot{m}_1 = \dot{m}_2$
Specific humidity	$SH_1 = SH_2$
Liquid water content	$CO_2 = \eta \cdot CO_1$

2.2 Treatment of humidity

Psychrometrics is the term used to describe the field of engineering concerned with the determination of physical and thermodynamic properties of gas-vapour. Knowing two properties of the moist air, the psychometric chart provides the others. Figure 4 shows how thermodynamic properties of moist air are represented on this chart.

As the humid air flows through the ECS its pressure and temperature fluctuate, which can lead to changes in humidity. The simulation uses a humidity algorithm (logic tree shown in Fig. 5) to calculate the magnitude of these changes. To this end, the humidity algorithm considers four possible scenarios:

i. No change in humidity
ii. Condensation
iii. Evaporation
iv. Evaporation until saturation

All of which are shown in the figure 5 logic tree.

Equations that are needed for the thermodynamic evaluation and the treatment of the humidity, as shown in Fig. 5, starting with the partial pressure of water vapour:

$$P_w = R_w T_{db} \rho_w \qquad (29)$$

Which at saturation, becomes:

$$P_{ws} = 610.78\, e^{17.2694\left(\frac{T_{db}}{T_{db}+238.3}\right)} \quad (30)$$

This feeds into the specific humidity, which is the ratio between the mass of the water vapour present in the moist air and the mass of the dry air.

$$SH = \frac{m_w}{m_a} = \frac{0.62198\, P_w}{(P - P_w)} \quad \text{Eq. 31}$$

From this the Specific Humidity at Saturation (SHS) is the mass of water per unit mass of dry air when air is saturated. The maximum amount of water vapour in the air is reached when P_w=P_{ws} and so:

$$\mathrm{SHS} = \frac{0.62198\, \mathrm{P_{ws}}}{(\mathrm{P} - \mathrm{P_{ws}})} \quad (32)$$

And relative humidity is:

$$\mathrm{RH} = \frac{\mathrm{SH}}{\mathrm{SHS}} \mathrm{x}\ 100 \quad (33)$$

The specific enthalpy of moist air (h) contains the total energy of both the dry air and water vapour per kilogram of air and the liquid water content per kilogram of air. It is expressed as:

$$\mathrm{h} = \frac{\mathrm{C_{pa}T_{db}} + \mathrm{SH}(\mathrm{C_{pw}T_{db}} + \mathrm{h_{fg}}) + \mathrm{CO}(\mathrm{C_{plw}T_{db}})}{(1 + \mathrm{SH} + \mathrm{CO})} \quad (34)$$

Gas constant is:

$$R = \frac{R_a + SH\, R_w}{1 + SH} \quad (35)$$

The specific heats of an air and water vapour mixture can be written in terms of the ratio of specific heats of air and water vapour mixtures and of the specific humidity.

$$C_p = \frac{C_{pa} + SH\, C_{pwv}}{1 + SH} \quad (36)$$

$$\gamma = 1 + \frac{R}{(C_p - R)} = \frac{C_p}{C_v} \quad (37)$$

2.3 Implemented simulation environment and interface

Having presented the component equations, the next step is to elaborate on how the overall simulation model is formed to represent a generic library of ECS components. The Matlab-Simscape environment was chosen for this purpose. The choice of software was based on a combination of factors that, amongst others, included: user friendliness, computational

effectiveness, flexibility in enabling further development and refinements, integration with other potential software platforms, and the ability to independently model each component performance coupled with its degradation modelling. All these prerequisites were deemed to be promising in making the decision to choose the Matlab Simscape environment.

Simscape offers the implementation of an object-oriented modelling approach, enabling a drag-and-drop interface, where each component can be independently formulated. This approach allows the flexibility to integrate the components together to represent the overall system, allowing the acquisition of system performance parameters at each component's inlet and outlet. Furthermore, this particular approach allows the construction of sub-libraries, e.g. a dedicated library can be assigned to represent faulty components, and the component design characteristics maps can be independently managed to ensure overall formulation is maintained universal and neat. Figure 6 illustrates the component sub-libraries formulated and scheduled to represent the overall SESAC library. The unique feature of constructing a generic library is to offer the user with the capability to construct any PACK architecture.

2.4 Compilation of the reference PACK Model

Figure 7 presents the compiled PACK model based on the SESAC library. The overall model mirror figure 3 and represents the PACK receiving input bleed air through the BAS at a specific T, P and $\dot{m}$, the quantity of which is controlled by the flow control valve, labelled as PV. The incorporated HPWS is represented as a sub-system composed of reheater, condenser and water extractor, allowing the extraction of water content prior to the expansion of the air in the turbine.

Once the expansion process is completed the air is mixed with the hot bypassed stream, controlled by the TCV. The merge component is incorporated to allow the mixing. The output temperature signal of the merge is controlled through a proportional integral derivative controller, which adjusts the TCV valve settings until the imposed target temperature is achieved. This process ensures that for any given operating condition, ait at the target temperature (cabin demand) is supplied to the mixing manifold system at the

demanded temperature. The TCV also enables prevention of ice formation in cases when the turbine outlet temperature drops below freezing.

The ram component is included to model the supply of cold air to the PHX and SHX. It should be noted that the control logic employed on the real aircraft in terms of RAM and TCV control is proprietary information. Therefore, the control logic used here is based on best engineering judgement and feedback received from industrial partners. The model control logic is same setup to match the primary PACK process parameters, i.e. allowing the ṁ is to vary in order to match the target T and P.

	Alt [ft]	Mach	Tamb [K]	Tamb [C]	Pamb [kPa]
Case 1	28000	0.761	232	-41	33
Case 2	41000	0.779	217	-56	18

2.5 Model boundary conditions

In order to systematically capture the performance of the overall PACK, boundary conditions must be appropriately defined throughout the model. These can be categorised in three ways: (i) aircraft state condition, (ii) bleed air properties and (iii) target output conditions.

The first part allows the model to determine the ram ṁ, which effectively serves as an input to the incorporated PHX and SHX cold streams. The model determines the ram ṁ based on the aircraft altitude, Mach number and the ram door total area and its percentage opening, this is done only if the aircraft state condition dictates that the aircraft is operating in flight. For ground operation, the model requires the ram ṁ and ambient temperature as an input to establish the cold stream ṁ for PHX and SHX. With regards to the second part, the model requires the bleed air properties in terms of P, T, specific humidity, and water content. Finally, the model requires the target conditions, i.e. T, P and ṁ. Table 1 presents the respective boundary conditions.

3. Results and Discussion

This section reports on the successful Verification and Validation (V&V) of the developed SESAC simulation. It presents the results acquired through running the simulation on two Boeing 737-800 PACK reference cases. The acquired results are corroborated against actual aircraft data. Furthermore, the characteristics of the key performance parameters, temperature, pressure and mass flow (T, P, and ṁ), are discussed for all PACK components.

Table 2: The two selected Reference Cases

3.1 Verification and Validation Methodology

To support the successful V&V of SESAC, two data sets, representing the performance characteristics of a Boeing 737-800 aircraft ECS, operating under steady state cruise conditions, have been employed. These two Reference Cases (RCs), shown in Table 2, are taken at different altitudes and provide data on T, P, and $\dot{m}$ throughout the PACK.

It should be noted that some discrepancy between the simulation and the system data is inevitable, which stems from : (i) the intrinsic wear and tear of the system, (ii) leakages present in system, and (iii) lack of accurate resolution of the system component performance map characteristics. The RCs include PACK losses not accounted for in the SESAC, e.g. component leakages and the losses associated with the interconnecting duct sealing leakages. Furthermore, the data may include some level of component fouling in the HXs, or losses in the mechanical efficiency of the ACM. Such losses are extremely difficult to account for in a physics based (theoretical) simulation unless real engineering insight of the system is available. Lack of such engineering knowledge of the system leads to inevitable discrepancies when comparing the simulation predictions against the actual data. As a consequence, and to support the discussion of the results, the SESAC simulation discrepancies in this study are referred to as the difference rather than the error between the SESAC prediction and the actual data.

The PACK model, shown in Figure 7, was run at the two conditions given in Table 2, and compared with the actual data in two main ways. First, the difference in the overall average values between the SESAC simulation and the validation data in terms of P, T and $\dot{m}$ throughout the PACK is presented and discussed. Then, the acquired simulation results in terms of P, T and $\dot{m}$ are compared with the validation data at component level with physical interpretation and analysis.

Three other points of simulation detail are worthy of note. First, the PACK V&V data corresponding to both RCs begins at the PV outlet, whereas the simulation begins at the PV inlet. As such, the PV inlet pressure (PVIP) was used to match the data's PV outlet pressure (PVOP) in the simulation. Second, in order to calibrate the temperature drop at the PHX and SHX outlet, the ram air door area is used to calibrate the simulation temperature at PHX and SHX outlet against the actual data in both cases. To summarise, each case is calibrated using the PVIP and ram air door area to align the simulation with the data. Finally, the V&V data is

collected at high altitude where the humidity is very low, therefore both cases were simulated assuming dry air.

3.2 Overall average differences

The relative difference between the simulation and the data is calculated from equation 39 for both RCs. This equation is applied to calculate the difference for P, T and ṁ at each component station between the simulation and the actual data throughout the PACK. The sum of the difference for these variables is then used to calculate the average difference for each parameter by using equation 40. Therefore, the average difference represents the overall difference between the simulation and data for the entire case for each parameter throughout the system.

Figure 8 shows the results for both RCs. From this the average difference between the simulation and the data in terms of P and T throughout the PACK is within 2% for both RCs, which is seen as good agreement. With regards to ṁ, the average difference is within 4% for both cases. The reasons for the simulation discrepancies with the actual data for all three parameters varies in the detail, e.g. for a given case the simulation may under or over predict the HX effectiveness, and in another case it may do the same for the air cycle machine. Also the ṁ difference is partly due to the data inlet and exit ṁ not being equal, due to seal losses. These, and other, points will be picked up in the next section.

$$Model\ Rel.\ Diff = \frac{(Model - actual\ data)}{actual\ data} \times 100\ [\%] \quad (39)$$

$$Model\ AVG\ Rel.\ Diff = \frac{\sum Model\ Rel.\ Diff\ at\ each\ station}{number\ of\ stations} \times 100\ [\%] \quad (40)$$

3.3 Reference Case 1 - Results and Discussion

Figure 9 presents the T, P, and ṁ corresponding to Reference Case 1 (RC1) against the simulation at component level throughout the PACK. Note that the stations labelled on the x-axis in Fig. 3 follow the sequence that is consistent with flow progression through the PACK, as annotated in Fig. 3.

It can be observed from Fig. 9 that the simulation exhibits good correlation with the data throughout the PACK. The P and T profiles capture the data trends across the PACK with an average difference of less than 2%. Note that, as elaborated earlier, the simulation is run using PVIP and ram door area as variables for calibration against the data.

It can also be seen from Fig. 9(b) that the difference between the simulated pressures and the data at PV Outlet (PVO) is around 2%, the corresponding PVOP of the simulation being adjusted to maintain the minimum difference through the remaining components of the PACK. If PVOP was further increased, it would result in shifting the pressure trend upwards and the entire pressure profile will move further away from the actual data. Therefore, for the approach adopted, in order to maintain a consistent match for the simulated pressure against the actual data throughout the PACK, some discrepancy in the PVOP has been accepted. It should be noted that only the PVIP was used to calibrate the PVOP, and through the remaining components of the PACK the pressure loss coefficients for the HXs (PHX, SHX, RHX, CHX) as well as the mechanical efficiency of the ACM, were maintained fixed throughout the simulation for both cases.

The calculated temperature profile shown in Fig. 9(a) is well matched with data throughout the PACK. In this case the PV outlet temperature from the data was imposed as the bleed air temperature at PV inlet and, as there is no temperature drop across the PV, this leads to a perfect outlet temperature match with the data. In terms of the calibration of the temperature for the remaining components, only the PHX outlet temperature was calibrated by iteratively adjusting the ram door percentage opening. On the real aircraft there is dedicated control logic which automatically adjusts the ram door flap settings in order to regulate the PHX and SHX performance, by controlling the amount of cold $\dot{m}$ supplied to the PHX and SHX. For the simulation, all of the HX effectiveness maps are incorporated within the model. These maps capture the effectiveness of the HXs as a function of the hot and cold mass flow supplied to the hot and cold streams of the HXs. From the simulation point of view, as mentioned earlier, the hot stream $\dot{m}$ for the PHX and SHX is determined based on matching the pressure conditions at the PVO. Therefore, the outlet temperatures of the PHX and SHX are calibrated based on the cold stream mass flow. This is done by adjusting the ram door inlet area.

Figure 9(a) shows that the temperature drop across the PHX and SHX matches the data very well. It implies that the simulation is able to match the point at which the PHX is operating on its performance map. Figure 10(a) shows a comparison of temperature drop across the PHX and SHX, calculated based on their respective inlet temperatures. For both PHX and SHX the simulation consistently matches the temperature drop with marginal discrepancy. Some of the discrepancy may be due to the actual data including losses associated with any fouling/blockage of the HXs or flow leakages.

Also, in Fig. 10(a) the comparison of the pressure drop across both the PHX and SHX is shown; the percentage values are calculated based on the inlet pressures to the PHX and the SHX respectively. The simulation shows good agreement with the data in terms of capturing the pressure drop of both the PHX and SHX, implying that the implemented HX pressure loss coefficients are accurate. It is interesting to note from Fig. 10(c) that the effectiveness of the PHX and SHX is between 86-87%, but that the effectiveness of the RHX and the CHX is significantly lower, around 56-60%.

The reason for this is that both the RHX and CHX are components of the HPWS, which is a sub-system of the PACK. The primary function of the HPWS is to remove water from the flow. To do this in a highly pressurised system like the PACK, the HPWS operates in the following way. After the SHX, the flow enters the RHX which fulfils multiple functions: (i) to cool the air flow prior to condensation, and (ii) to reheat it prior to the expansion in the turbine. As such, the cold stream of the reheater is represented by the flow received from the outlet of the water extractor, which needs to be heated before it is supplied to the turbine, and the hot stream is represented by the flow received from the outlet of the SHX, which needs to be cooled before it is supplied to the condensers. The temperature difference between both of these stream is very small, which leads to very limited exchange of heat between the both streams, hence resulting in low effectiveness relative to the PHX and the SHX which exploit very cold ram air for cooling. In a similar fashion to RHX, the CHX further cools the flow supplied by the reheater in a hot stream and heats the flow after the merger in the cold stream, just before it is supplied to the Mixing Manifold System (MMS).

With regards to the simulation comparison for the compressor, inlet conditions for the compressor are based on the PHX outlet conditions. From Fig. 9 note that for the simulation, the inlet temperature for the compressor is slightly higher and the inlet pressure is marginally lower relative to the data. Figure 10(b) shows the comparison of the temperature and pressure rise between the simulation and the data across the compressor. For both parameters the simulation over predicts the data. One possible reason for this over prediction is that in the ACM the compressor and turbine are mounted on the same shaft, and the balance between the compressor and the turbine work is based on their mechanical efficiency. It could be that the ACM mechanical efficiency used in the simulation is not consistent with the actual data. This would be a very difficult parameter to measure.

Moving on to the RHX, CHX and WS. As elaborated earlier, all three components are interconnected and assembled as one module (HPWS), and can therefore be represented as a sub-system of the PACK, its functionality enabling water content to be removed at high pressure. Since the validation data does not include the humidity, validation for water content/humidity of the simulation has not been implemented under the scope of this study, and will not be discussed further. Once the water content from the flow is removed the flow is supplied to the turbine through the RHX.

The key purpose of the turbine in this system is to drop the temperature of the flow, and generate the shaft power required to support the compression. The turbine therefore expands the flow primarily to enable the PACK to condition the flow to match the temperature requirement, in this process the pressure of the flow drops too. In some cases the turbine outlet temperature can drop below freezing. A merge component is mounted immediately downstream of the turbine which allows the mixing of the turbine outlet flow with the bypassed bleed air. The bleed air supply to the merge is controlled by the temperature control valve. The merge component therefore allows the adjustment of the turbine outlet temperature to match the target PACK outlet temperature.

With regards to the acquired $\dot{m}$ results, it can be noticed from Fig. 9(c) that the simulation exhibits good correlation with the data in terms of capturing the key characteristics of the system. The total $\dot{m}$ at the PVO is split into two steams: (i) bypass bleed air which is controlled by the TCV as a hot stream, (ii) a cold stream that runs through the core of the PACK (Fig. 3). The sudden drop in the $\dot{m}$ after the PV is because the PACK flow is being plotted and hence the flow drops from 0.43 to 0.31; in this case the hot stream represents around 27% of the total mass flow at PVO. This hot stream re-joins the cold stream at the merge in order to combine with the turbine outlet temperature to meet demand. This remerging process of the flow is shown by the rise in $\dot{m}$ to reach its original value, since the simulation does not account for any leakages. However, this is not the case for the data, as can be seen from Fig. 9(c) where the mass flow at the PACK Outlet (PO) is slightly lower relative to the PVO value, by approximately 3%. This implies that the data contains the effect of leakages in the components or in the seals, used to connect the various components throughout the PACK. The fact that the simulated $\dot{m}$ profile is lower than the data is due to the dependence of the PVO $\dot{m}$ on the PVOP, as previously discussed.

To illustrate the dependency of the profiles on the value of PVOP, the data value of outlet ṁ has been matched by the simulation, and the results are presented in Fig 11. In these graphs the previous case has retained its designation (SESAC), along with the actual data, the new results (target ṁ) have been superimposed. As expected, the pressure profile for the target ṁ match simulation moves further away from the actual data than the PVOP match previously discussed. The temperature profile is almost completely unaffected. Summarising, there are two possible solutions that the model can generate in terms of matching the data: (i) run the model to match the PVOP providing a good correlation for the pressure profile across the system, (see Fig. 9), (ii) run the model to achieve the target ṁ match (see Fig. 11). In the former case the compromise is in average ṁ difference, and in the latter case a compromise in the pressure difference must be accepted. This is summarised in Fig.12, when the simulation is run to match the PVOP conditions, the average relative difference between the simulation and the data for pressure is less than 1.5%. However, the ṁ difference is significantly higher, around 4%. In the case when the simulation is run to match the target ṁ, the average ṁ difference drops from 3.94% down to 1.34%, with a compromise of doubling the average pressure difference relative to the data. The simulation can accommodate either assumption.

3.4 Reference Case 2 – Results and Discussion

The results of running the simulation on Reference Case 2 (RC2) are presented in Fig. 13. As for RC1, the predictions for T, P, and ṁ are in good agreement with the data throughout the PACK. For both RCs the simulation consistently captures the characteristics of each component, demonstrating that the PACK performance can be simulated for any given aircraft operating point. The difference between the data and the simulation for RC2 is less than 1.3% for T and P throughout the PACK, and less than 3.7% for ṁ. The fundamental potential reasons leading to the simulation discrepancies remain the same as highlighted and discussed for RC1 in Section 3.3.

Before going into detail on the comparison between the two cases, a note on the effect of the change in ambient is appropriate. Table 2 summarised the two cases, with RC2 being at a higher altitude. The Mach number is essentially the same for both cases, but the change in ambient pressure and temperature is significant. At altitudes equal to and above 8000ft, the

aircraft is required to maintain cabin pressure equal to 8000ft altitude (78-80kPa). With a falling outside pressure, bleed air is extracted from the engine compressor at different stages to maintain a constant inlet pressure to the PACK. As pressure and temperature rise together through the compressor the PACK inlet temperature will also be very close for both cases. However, for RC2, at the higher altitude, with a lower outside temperature, considering a heat balance over the aircraft, the cabin temperature demand will rise. The data confirms this as, (Fig. 13), with an increase in cruising altitude, the demanded outlet temperature from the PACK changes from 291K – 298K (18°C - 25°C).

When comparing the temperature profile of both cases, it is apparent from Fig. 13(a) that the temperature drop through the primary and secondary heat exchangers is significantly different between both cases. This is due to the local ambient temperature and pressure difference affecting the density and hence the mass flow through the ram intake. The local air properties are presented in Table 3.

Due to the drop in the ram $\dot{m}$, the PHX cold mass flow changes by nearly 50% between the two cases. With less mass flow through the RC2 intake, the heat exchanged with the hot engine bleed has been reduced and the air emerging from the PHX is hotter. Only after compression and subsequent cooling through the SHX does the temperature drop to the required level. Both heat exchangers are acting more in unison at the higher altitude. Figure 14(a) confirms these temperatures changes and Fig. 14(b) shows the comparison of the PHX effectiveness between both cases. A clear drop in the PHX effectiveness is apparent for RC2, and can be attributed to the differences in the amount of cold and hot mass flow passing through the PHX in each case. Further, the $\dot{m}$ of the PHX hot stream is represented by the results shown in Fig. 11(c) for RC1 and Fig. 13(c) for RC2. The station PHX Outlet (PHXO) represents the $\dot{m}$ of the PHX hot stream. Relative to RC1, RC2 has approximately 5% less $\dot{m}$ flow running through its PHX hot stream, due to the higher cabin demand temperature.

Comparing PHX, compressor and SHX performance, different conclusions can be reached for RC1 and RC2. For RC1 both the PHX and compressor performance exactly lines up to the data, while for RC2 it is the SHM performance that looks different. Therefore, with only the data shown here it would be impudent to alter any of the component modelling. The simulations provide valuable insights and point to physical phenomena that are plausible;

clearly more data and simulation experience is needed to claim a mature simulator. The development of a ground test facility targeting full scale condition monitoring of an aircraft ECS is currently underway at Cranfield University [7]. Its successful completion will enable comprehensive data collection and will therefore facilitate a robust verification and validation of the simulation.

Conclusions

In this paper a computationally efficient, cost effective and robust simulation framework called SESAC- Simscape Environmental Control System Simulation under All Conditions has been proposed and implemented. The innovative contributions of this research paper are:

- Formulation and development of a simulation framework for the performance evaluation of an aircraft environmental control system operating under a wide range of functional scenarios.
- Simulation of a Boeing 737-800 aircraft passenger air conditioner and its verification and validation against actual data at sub-system and component level.
- Quantification of the performance characteristics and the component level interdependencies of the PACK at various aircraft cruise operating points.
- The quantification of the impact of ram air sensitivity on the PACK overall performance.

An extensive comparison of the simulation is presented against the data in terms of temperature, pressure and mass flow throughout the aircraft passenger air conditioner. The verification and validation has been carried out against the actual data corresponding to a Boeing 737-800 aircraft operating at two different cruise operating points.

The overall results suggest that the change in the aircraft ambient conditions can have noticeable impact on the demanded passenger air conditioner outlet temperature, and a substantial impact on the heat transfer capability of the primary and secondary heat exchangers.

Finally it has been emphasized that a relatively small change in the boundary conditions can cause a large impact on the performance of the passenger air conditioner components. The simulation sufficiently capture the component characteristics and interdependencies that proof significant value towards advancing the level of scientific understanding of the environmental control system.

References

1. H. Elwood., R. R. David. T. Fred, Commercial airliner environmental control system: engineering aspects of cabin air quality, The Boeing Company, Aerospace Medical Association annual meeting, Anaheim, California, May 1995.
2. I. Jennions, Integrated Vehicle Health Management Perspectives on an Emerging Field. Warrendale, PA: SAE International; 2011.
3. M. Esperon. P. John. I. Jennions, A review of Integrated Vehicle Health Management tools for legacy platforms: Challenges and opportunities, Progress in Aerospace Sciences, Volume 56, 2013, 19-34.
4. C. Ezhilarasu. Z. Skaf. I. Jennions, Application of Reasoning to Aerospace Integrated Vehicle Health Management (IVHM): Challenges and Opportunities", Progress in Aerospace Sciences, Volume 105, 2019, 60-73.
5. H. Lightfoot. M. Greenough, State-of-the-art in integrated vehicle health management State-of-the-art in integrated vehicle health". 2016 1–14.
6. C. Escobar, Condition Monitoring For Environmental Control Systems. MSc Thesis, Integrated Vechicle Health Management, Cranfield University; Octotber 2015.
7. C. Shafayat. F. Ali. I. Jennions, A Methodology for the Experimental Validation of an Aircraft ECS Digital Twin Targeting System Level Diagnostic, proceedings of annual conference of the prognostics and health management society 2019, 11th PHM Conference, Scottsdale, AZ, USA, September 21-26.

8. I. Grande. T. Leo, Optimisation of a commercial aircraft environmental control system, Appl. Thermal. Eng. 22 (2002) 1885 - 1904.
9. T. Leo. I. Grande, A thermoeconomic analysis of a commercial aircraft environmental control system, Appl. Thermal. Eng. 25 (2005) 309 - 325.
10. H. Zhao. Y. Hou. Y. Zhu. L. Chen. S. Chen, Experiential study on the performance of an aircraft environmental control system, Appl. Thermal. Eng. 29 (2009) 3284 - 3288.
11. S. Wright. G. Andrews. H. Sabir, A review of heat exchanger fouling in the context of aircraft air-conditioning systems, and the potential for electrostatic filtering, Appl. Thermal. Eng. 29 (2009) 2596 - 2609.
12. K. Palmer. W. Hale. K. Such. B. Shea. G. Bollas, Optimal designs of tests for heat exchanger fouling identification, Appl. Thermal. Eng. 95 (2016) 382 - 393.
13. H. Yang. X. Zhang. C. Wang. C. Yang, Experimental and theoretical study on a novel energy-saving ECS for commercial airlines, Appl. Thermal. Eng. 127 (2017) 1372 - 1381.
14. D. Cholz. T. Giese. C. Erdmann, FLECS : Functional Library of the Environmental Control System – A simulation Tool for the support of Industrial Processes, AST 2007, March 29-30, Hamburg, Germany. 2007.
15. C. Müller. D. Scholz, Dynamic simulation of innovative aircraft air conditioning, 1st CEAS European Air and Space Conference. 2007. pp. 869–878.
16. Tu. Y G. Lin, Dynamic Simulation of humid air environmental control system, 40th International Conference on Environmental Systems. 2010. pp. 1–10. Available at: DOI:10.2514/6.2010-6305
17. Tu. Y., Lin P., "Dynamic simulation of aircraft environmental control system based on flowmaster", Journal of Aircraft. 2011, 48(6): 2031–2041.
18. X. Lang. P. Li. Z. Hu. H. Ren, L. Yan, Leak Detection and location of pipelines based on LMD and least squares twin support vector machine, IEEE, 20178659–8668.
19. D. Burroughs. A. Hammond, Control analysis and design features of EASY5". American Control Conference. San Francisco; 1983. pp. 58–63.
20. G. Hoffman, Environmental control system Simulation using EASY5, as applied to the F-14, Intersociety Conference on Environmental Systems. 1985.
21. C. Schooley, A Time-response analysis of an air distribution subsystem of an aircraft environmental control system using Easy5". MSC.Software VPD Conference. 2006.
22. J. Karlsson, Diagnosis of the air distribution system of the JAS39 Gripen environmental control system. Linköping Institute of Technology; 2001.

23. R. Romani, Cabin temperature control model for commercial aircraft", Modeling and Simulation Technologies Conference. 2012, 1–15.
24. C. Smith, Calculation of flow of air and diatomic gases," Journal of the Aeronautical Sciences. 1994, 309–315.
25. J. Hesselgreaves, Compact heat exchangers: selection, design and operation, Elsevier, 1st Edition. ISBN**:** 9780080529547.

Fig. 1. Major sub-systems of a typical civil aircraft ECS [1].

Fig. 2. Aircraft ECS key sub-systems block diagram.

Fig. 3. Component level schematic of the B737-800 PACK with labelling of the air flow sequence.

Fig. 4. Properties of moist air on a psychrometric chart (SH= specific humidity [kg/kg], RH= relative humidity [%], Tdb =Dry bulb temperature [K], h= enthalpy.

Fig. 5. Humidity treatment

Fig. 6. The developed SESAC component library.

Fig. 7. SESAC PACK model corresponding to the reference B737-800 aircraft configuration.

Fig. 8. The average difference between the simulation and the data for both RCs.

Fig. 9. Reference Case 1: temperature, pressure and mass flow distributions throughout the PACK.

Fig. 10. Comparison of the SESAC simulation and the data: (a) and (b) the ΔT and ΔP across the PHX, SHX and compressor, the labels also show actual values in standard units at outlet of each station, (c) simulation prediction for the component effectiveness/efficiencies.

Fig. 11. Reference Case 1: comparing results between matching PVOP and matching mass flow as alternative boundary conditions.

Fig. 12. Reference Case 2 results: comparison of differences for SESAC simulations based on matching PVOP or matching target mass flow as alternative boundary conditions.

Fig. 13. Reference Case 2: temperature, pressure and mass flow comparisons throughout the PACK.

Fig. 14. Comparison of various performance parameters between RC1 and RC2; (a) ΔT across PHX, SHX, compressor and turbine, the labels also show actual values in standard units at outlet of each station, (b) effectiveness and efficiency of PHX, SHX and ACM.

Table 1. Required input boundary conditions to simulate the PACK performance in the developed simulation model.

Component	**Parameters**	**Description**	**Units**
Aircraft State condition	Selector (S)	Determines if the aircraft is in flight or operating at ground static conditions. 1= inflight, 0 = ground static.	[-]
Ram (0: Ground Static)	$\dot{m}$	Ram $\dot{m}$ is required if aircraft operating at ground static.	[-]
	T_{amb}	Ambient temperature	[K]
Ram (1: In flight)	Alt	Aircraft Altitude	[m]
	Mach	Aircraft Mach number	[-]
	Area	Ram door total area	[m^2]
	%Open	Ram door opening in %	[%]
Bleed Air properties			
	T_{BAS}	Inlet temperature to PV	[K]
	P_{BAS}	Inlet pressure to PV	[Pa]
	SH_{BAS}	Inlet specific humidity at PV	[kg/k]
	CO_{BAS}	Inlet liquid water content at PV	[kg/k]
Target Conditions	P_{cab}	Cabin pressure – $PACK_{outlet}$	[Pa]
	T_{cab}	Cabin pressure – $PACK_{outlet}$	[K]
	$\dot{m}_{cab}$	Cabin pressure – $PACK_{outlet\dot{m}}$	[kg/s]
Parameter(s) used as handle			
PVIP	P_{BAS}	Inlet pressure to PV	[Pa]
Ram	%Open	Ram door opening in %	[%]

Table 3. Reference case 1 and 2 local air properties and Ram inlet mass flow.

	T_{amb} [K]	P_{amb}[kPa]	ρ_{amb} [kg/m^3]	Ram $\dot{m}$ [kg/m^3]
RC1	232.65	32.94	0.49	0.40
RC2	216.65	17.79	0.29	0.21

2020-01-09

Simulation of an aircraft environmental control system

Jennions, Ian

Elsevier

Jennions I, Ali F, Esperon Miguez M, Camacho Escobar I. (2020) Simulation of an aircraft environmental control system. Applied Thermal Engineering, Volume 172, May 2020, Article number 114925

https://doi.org/10.1016/j.applthermaleng.2020.114925